Systems/Circuits

Encoding of Environmental Cues in Central Amygdala Neurons during Foraging

Marion Ponserre,* Federica Fermani,* Louise Gaitanos, and Rüdiger Klein
Department of Molecules–Signaling–Development, Max Planck Institute for Biological Intelligence, in foundation, Martinsried Am Klopferspitz 18, 82152 Planegg, Germany

To successfully forage in an environment filled with rewards and threats, animals need to rely on familiar structures of their environment that signal food availability. The central amygdala (CeA) is known to mediate a panoply of consummatory and defensive behaviors, yet how specific activity patterns within CeA subpopulations guide optimal choices is not completely understood. In a paradigm of appetitive conditioning in which mice freely forage for food across a continuum of cues, we found that two major subpopulations of CeA neurons, Somatostatin-positive (CeA^{Sst}) and protein kinase Cδ-positive ($CeA^{PKC\delta}$) neurons, can assign motivational properties to environmental cues. Although the proportion of food responsive cells was higher within CeA^{Sst} than $CeA^{PKC\delta}$ neurons, only the activities of $CeA^{PKC\delta}$, but not CeA^{Sst}, neurons were required for learning of contextual food cues. Our findings point to a model in which $CeA^{PKC\delta}$ neurons may incorporate stimulus salience together with sensory features of the environment to encode memory of the goal location.

Key words: **associative memory; central amygdala; foraging; miniscope calcium imaging; optogenetic; reward learning**

Significance Statement

The CeA has a very important role in the formation of memories that associate sensory information with aversive or rewarding representation. Here, we used a conditioned place preference paradigm, where freely moving mice learn to associate external cues with food availability, to investigate the roles of CeA neuron subpopulations. We found that CeA^{Sst} and $CeA^{PKC\delta}$ neurons encoded environmental cues during foraging but only the activities of $CeA^{PKC\delta}$ neurons were required for learning of contextual food cues.

Introduction

The survival of an animal depends heavily on its ability to evaluate whether familiar cues in the environment predict a threat or an opportunity. The CeA is important for this competence and contains numerous genetically distinct subpopulations of neurons that can select the appropriate behavioral outputs in the face of positively or negatively valenced stimuli (Ehrlich et al., 2009; Pare and Duvarci, 2012; Herry and Johansen, 2014; Janak and Tye, 2015; Fadok et al., 2018). Although earlier models interpreted the literature in a binary mode, where CeA neurons belong either to the aversive or rewarding network, new hypotheses depict the CeA as an essential site for associative learning (Wilensky et al., 2006; Ciocchi et al., 2010) also contributing to the computation of prediction error signals (Ozawa et al., 2017; Yu et al., 2017; Kargl et al., 2020). To understand how the surrounding environment modulates plasticity in CeA circuits to drive behavioral selection, we probed the function and activity patterns of $CeA^{PKC\delta}$ and CeA^{Sst} neurons during a foraging task. PKCδ- and Sst-expressing cells represent two nonoverlapping populations of CeA neurons (Kim et al., 2017), encompassing the majority of all cells in this region (Kim et al., 2017), and are known to mediate antagonizing behaviors when studied in parallel (Kim et al., 2017; Wilson et al., 2019; Kargl et al., 2020). The CeA has been previously shown to acquire responses to signals of food delivery, but the contribution of these two CeA subpopulations has remained unclear (Gallagher et al., 1990; Han et al., 1997, 1999; McDannald et al., 2004; Corbit and Balleine, 2005; Lee et al., 2005). In particular, how these appetitive memories are represented in a setting where the animal freely navigates and is forced to engage in goal-oriented actions remains unknown. We hypothesized that PKCδ+ cells that integrate convergent inputs from cortical, thalamic, hippocampal, and brainstem structures (Douglass et al., 2017), properties that are reminiscent of the Hebbian model of learning-

Received Sep. 1, 2021; revised Feb. 3, 2022; accepted Mar. 8, 2022.

Author contributions: M.P., F.F., and R.K. designed research; M.P., F.F., and L.G. performed research; M.P. and F.F. analyzed data; M.P. and R.K. wrote the paper.

This work was supported by the Max-Planck Society, the Deutsche Forschungsgemeinschaft (Grant SPP1665), and the European Research Council under the European Union Horizon 2020 Research and Innovation Program (Grant No. 885192). We thank Nejc Dolensek, Aljoscha Leonhardt, Matthias Meier, and Ruben Portugues for help with data analysis and Jorge Cotino and Yanis Pignot for help with management of the animal colony.

*M.P. and F.F. contributed equally to this work.

The authors declare no competing financial interests.

Correspondence should be addressed to Rüdiger Klein at rklein@neuro.mpg.de.

https://doi.org/10.1523/JNEUROSCI.1791-21.2022

induced synaptic plasticity, may be involved in associative learning tasks that impose valence on different tastes or link taste valence to other sensory stimuli.

Indeed, we found that CeA$^{PKC\delta}$ neurons, previously related to aversive behavior (Haubensak et al., 2010; Cai et al., 2014; Cui et al., 2017; Kim et al., 2017; Yu et al., 2017; Wilson et al., 2019), were required for approach behavior in a context that signals food availability, whereas CeA^{Sst} neurons were not. We performed Ca^{2+} imaging to evaluate neuronal activity changes when the mice freely decided to switch between environments. We observed that after learning, a subset of these two populations had developed specific activities to the positive context. Our findings suggest a model in which CeA^{Sst} neuron activity encodes information directly related to food consumption, whereas CeA$^{PKC\delta}$ cells endow sensory features of the environment with representation of the food reward salience to ultimately drive correct behavioral choices.

Materials and Methods

Animals

Prkcd-Cre (Tg(Prkcd-glc-1/CFP,-Cre)EH124Gsat) BAC mice were imported from the Mutant Mouse Regional Resource Center. *Sst-Cre* (Ssttm2.1(cre)Zjh) transgenic mice were acquired from The Jackson Laboratory (https://www.jax.org/). Rosa26R Cre-dependent reporter mice that express LacZ (B6.129S4-Gt(ROSA)26Sortm1Sor/J) have been described previously (Soriano, 1999). Mice were backcrossed onto a C57BL/6NRj background (Janvier Labs; http://www.janvier-labs.com). Three- to 6-month-old male *Prkcd-cre;LacZ* or *Sst-Cre;LacZ* mice were used for the place preference assay combined with optogenetic manipulation of CeA$^{PKC\delta}$ and CeA^{Sst} cells, as well as for the open field task. Eight- to 18-month-old male and female *Prkcd-cre;LacZ* or *Sst-Cre;LacZ* mice were used for the place preference assay combined with Ca^{2+} imaging of CeA$^{PKC\delta}$ and CeA^{Sst} cells. The older age of mice used for the Ca^{2+} imaging experiments was primarily because of the experimental design. In some cases, a waiting period of several months was necessary for the inflammation to decrease and to clearly see fluorescent cells through the lens. Mice were kept on a 12 h light/dark cycle. All behavior experiments were conducted during the light phase of the cycle and under dimmed light in the behavioral boxes.

Viral constructs

The following adeno-associated viruses (AAVs) were purchased from the University of North Carolina Vector Core (https://www.med.unc.edu/genetherapy/vectorcore): AAV5-ef1a-DIO-eNpHR3.0-mCherry and AAV5-ef1a-DIO-mCherry. The AAV5-Syn.Flex.GCaMP6s virus was obtained from Addgene (http://www.addgene.org/).

Stereotaxic surgeries

Viral injections in the CeA. Mice were anaesthetized using isoflurane (induction, 3%; maintenance, 1.5%; CP-Pharma) in oxygen-enriched air and head fixed on a stereotaxic frame (model 1900, Kopf Instruments). Body temperature was maintained at 37°C using a heating pad. Carprofen (Rimadyl, 5 mg/kg body weight; Zoetis) and an analgesic, were given via subcutaneous injection. Mice were bilaterally injected with 0.3 µl of virus in the CeA by using the following coordinates calculated with respect to the bregma: −1.22 mm anteroposterior, ±2.9 mm lateral, −4.7 to −4.8 mm ventral. Viral particles were delivered using glass pipettes (catalog #708707, Blaubrand intraMark) connected to a Picospritzer III (Parker Hannifin) and controlled by a Master-8 pulse stimulator (AMPI) at a flow rate of ~50 nl/min. After delivery of the virus, the pipette remained in the brain for 5 min to prevent spread of the virus. Virus was allowed to be expressed for a minimum duration of 4.5 weeks and a maximum of 10 weeks before behavioral experiments.

Optic fiber implants. Mice used in optogenetic experiments were, in the same surgery, bilaterally implanted with optic fibers (200 µm core, 0.22 NA, 1.25 mm ferrule; Thorlabs) above the CeA (−4.35 mm ventral from bregma). The skull was first protected with a thin layer of histo glue (Histoacryl, Braun), the fibers were then fixed to the skull using UV light-curable glue (Loctite, catalog #AA3491, Henkel), and the exposed skull was covered with dental acrylic (Paladur, Heraeus).

Gradient index lens implantation and baseplate fixation. For gradient index (GRIN) lenses implantation, 3 weeks after viral injection, mice expressing GCaMP6s in PKCδ+ or SST+ cells were anesthetized using the same procedure as described above. A small craniotomy was made above the CeA using the same coordinates as for the injection of the viral preparation. Debris were removed from the hole, and a customized blunted 23G needle (0.7 mm in diameter) was slowly lowered down into the brain at a speed of 150 µm/min to a depth of −4.6 mm from bregma. After retraction of the needle, a GRIN lens (ProView Lens; diameter, 0.5 mm; length, ~8.4 mm; Inscopix) mounted on a GRIN lens holder was slowly (150 µm/min) implanted above the CeA. The skull was first protected with a thin layer of histo glue (Histoacryl, Braun), and the lens was then fixed to the skull using UV-light-curable glue (Loctite, catalog #AA3491, Henkel), and the exposed skull was covered with dental acrylic (Paladur, Heraeus). The exposed top of the lens was protected by a covering of a silicone adhesive (Kwik-Cast, World Precision Instruments). Four to 8 weeks after GRIN lens implantation, mice were anesthetized and placed in the stereotaxic setup. A baseplate (BPL-2, Inscopix) attached to the miniature microscope was positioned above the GRIN lens. Concentration of the anesthetic gas was lowered, and the focal plane was adjusted until neuronal structures and GCaMP6s dynamics were clearly observed. Mice were then fully anaesthetized again and the baseplate was fixed using C&B Metabond (Parkell). A baseplate cap (BCP-2, Inscopix) was left in place until imaging experiments.

Behavioral assays

Conditioned place preference with food reward. The conditioned place preference behavior was motivated by previous work (Stern et al., 2018). It was conducted in a custom-built arena made of two chambers: a rectangular-shaped chamber (45 * 15 cm) and a triangular-shaped chamber (45 * 30 cm) separated by a corridor (Fig. 1*A*). Chambers additionally differed based on the texture of the floor and pattern on the walls. The area size of the two chambers was identical. On the first day of the behavioral experiment, mice were allowed to explore the arena for 20 min. Preferences for the two chambers were measured, and the least preferred one was chosen as the food-paired chamber (+ context) for the rest of the paradigm. From then on, and until the end of the experiment, mice were singly housed and food restricted. They were weighed daily and supplied with necessary food to maintain at least 85% of their initial body weight. Conditioning was then conducted over 4 consecutive days. For this, mice were first sequestered in the neutral context for 15 min and then manually transferred to the positive context for 15 min in which they had access to a food pellet of ~1 g. The remaining food was weighed at the end of each conditioning session to determine food consumption. On the fifth and final day of the experiment, mice were allowed to freely navigate between the two chambers in the absence of food. The preference for the positive context was measured for a period of 10 min as a readout for contextual appetitive conditioning. For Ca^{2+} imaging experiments, mice were subjected to the same behavioral task, and at the end of the 10 min recall session, we added a food pellet to the positive context and recorded the activity of CeA cells for another 10 min.

We had previously performed pilot experiments with WT animals in which three groups of five mice were conditioned either for 2, 4, or 5 d, and the preference of each group for the positive chamber was tested 24 h after the last conditioning day. We found that preference for the appetitive chamber increased from 53.6% ± 1.3 to 71.9% ± 7.6 when we increased the conditioning from 2 to 4 d but did not increase further when performing the experiment for 5 conditioning days [preference index (PI) = 61.7% ± 5; data not shown]. We therefore chose to perform 4 d of conditioning because a preference of 70% for the food-paired chamber would give us a perfect range to identify both increases and decreases in our optogenetic experiment. In our imaging experiment, we also needed animals that would move a lot between the two chambers and spend a sufficient amount of time in both contexts so that we could

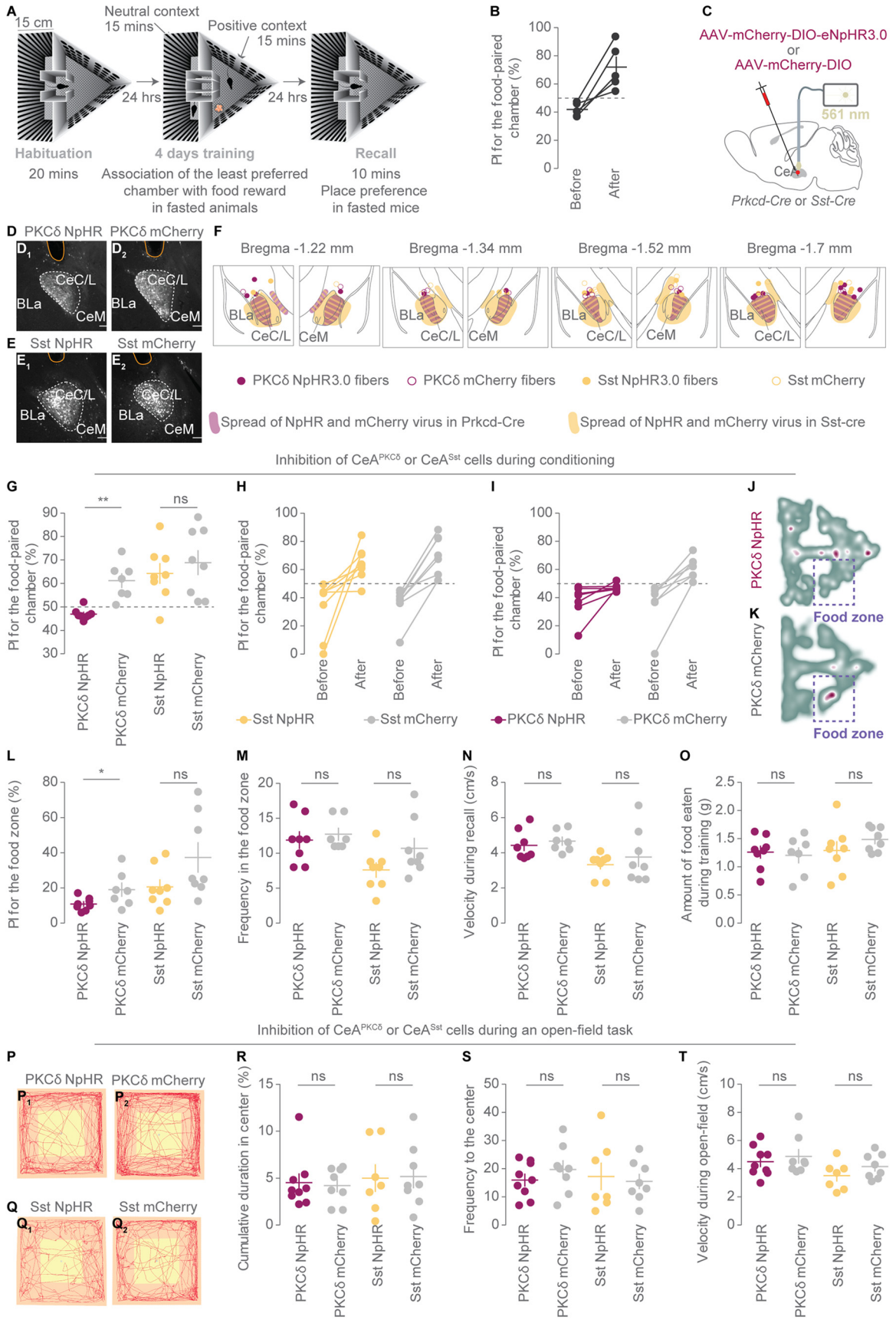

Figure 1. Inhibition of CeA$^{PKC\delta}$ neurons during conditioning impairs contextual appetitive conditioning. ***A***, Place preference behavioral paradigm. ***B***, PI for the positive context before and after conditioning for WT animals ($n = 5$ mice). ***C***, Optogenetic inhibition of CeA neurons. The CeA of Prkcd-Cre or Sst-Cre mice was transduced with a Cre-dependent AAV-expressing eNpHR3.0-mCherry or mCherry alone. CeA neurons were photoinhibited *in vivo* with constant yellow light. ***D***, ***E***, Representative epifluorescent images of Prkcd-Cre (***D***) and Sst-Cre mice (***E***) injected in the CeL with an AAV-DIO-eNPHR3.0-mCherry (***D$_1$***, ***E$_1$***) or AAV-DIO-mCherry (***D$_2$***, ***E$_2$***) and showing the location of the optic fiber tract (in yellow). Scale bars: 100 µm. ***F***, Approximate optic fiber

see both an increase in activity in the positive chamber and a decrease in activity in the neutral one.

For the optogenetic experiments, PKCδ-eNpHR3.0, PKCδ-mCherry, Sst-eNpHR3.0 and Sst-mCherry mice bilaterally received constant 561 nm intracranial light (15 mv) either during the whole 30 min of the conditioning (both in the positive and neutral context) and during all four conditioning sessions, or during the whole recall session only. For this, mice were tethered to optic-fiber patch cables (Doric Lenses or Thorlabs) connected to a 561 nm Changchun New Industries laser (Hübner) via a rotary joint (Doric Lenses) and mating sleeve (Thorlabs). During habituation and recall, mice were free of the optic-fiber patch cables.

Animals that did not explore both chambers at least once during recall were excluded. This includes 1 PKCδ-eNpHR3.0, 1 PKCδ-mCherry, and 1 Sst-eNpHR3.0 animals used for the experiment in Figure 1, *G* and *O*, and 1 PKCδ-eNpHR3.0, 1 Sst-mCherry, and 2 Sst-eNpHR3.0 animals used for the experiment in Figure 3.

Open field. PKCδ-eNpHR3.0, PKCδ-mCherry, Sst-eNpHR3.0, and Sst-mCherry mice were allowed to explore a custom-built Plexiglas arena (40 cm × 40 cm × 25 cm) for 10 min. During the experiment, mice bilaterally received constant 561 nm intracranial light through optic-fiber patch cords (Doric Lenses or Thorlabs) connected to a 561 nm Changchun New Industries laser (Hübner) via a rotary joint (Doric Lenses) and mating sleeve (Thorlabs).

Real-time place preference. Real-time place preference (RTPP) assays were conducted over 2 consecutive days. On the first day, PKCδ-eNpHR3.0 and PKCδ-mCherry mice were allowed to explore a custom-built arena made of two chambers (25 * 25 cm each) for 20 min. Mice received constant 561 nm intracranial light in one chamber, the photoinhibition-paired chamber. The laser was triggered on the basis of the location of the animal by using EthoVision XT 14 software (Noldus). On the next day, the experiment was repeated under the same conditions as on day 1, except that the photoinhibition-paired chamber was switched.

Conditioned place preference without food reward. Conditioned place preference experiments without food reward were conducted in a similar manner as conditioned place preference experiments with food reward except that the inhibition of $CeA^{PKC\delta}$ neurons was not paired with delivery of a food reward. Briefly, the experiment was conducted in a custom-built square arena (26.5 × 26.5 cm), divided in the middle by a wall with an opening to form two equally sized triangular compartments that the mice could freely navigate between. Chambers differed based on the texture of the floor. On the first day of the behavioral experiment, PKCδ-eNpHR3.0 and PKCδ-mCherry mice were allowed to freely explore the arena for 20 min. Preferences for the two chambers were measured, and the least preferred one was chosen as the photoinhibition-paired chamber for the rest of the paradigm. Conditioning was then conducted over 4 consecutive days in which mice were sequestered for 15 min in each chamber but received constant 561 nm intracranial light only in the photoinhibition-paired chamber in the absence of food. On the fifth and final day of the experiment, mice were able to freely navigate between the two compartments, and the preference for the photoinhibition-paired chamber was measured over a 20 min period.

In vivo Ca^{2+} imaging of freely moving mice

All imaging experiments were conducted on freely behaving PKCδ-GCaMP6s and Sst-GCaMP6s mice. GCaMP6s fluorescence signals were acquired using a miniature integrated fluorescence microscope system (nVoke, Inscopix). Before each imaging session, the miniscope was secured in the baseplate holder. Mice were habituated to the miniscope attachment procedure 3 d before behavioral experiments. The analog gain and LED output power were adjusted so that the best dynamic fluorescence signals were at the focal plane. Settings were kept constant within subjects and across imaging sessions. Imaging acquisition and behavior were synchronized using the data acquisition box of the nVoke Imaging System (Inscopix), triggered by the EthoVision XT 14 software (Noldus) through a transistor–transistor logic box (Noldus) connected to the USB-IO box from the EthoVision system (Noldus). Compressed images were obtained at 1200 pixels × 800 pixels and 10 frames per second using the Inscopix acquisition software. We recorded the activities of CeA neurons during habituation on day 1 and day 3 of conditioning and during recall. To minimize photobleaching, we limited the duration of acquisition to three times for 2 min during habituation, 1 time for 2 min during conditioning in the neutral context, and three times for 2 min during conditioning in the positive context. Each recording bout was evenly spaced in time. On recall day, Ca^{2+} transients were recorded for the full 20 min of the behavioral experiment.

Histology

Animals that underwent behavioral experiments combined with optogenetic manipulations of CeA cells were anesthetized with ketamine/xylazine (100 mg/kg and 16 mg/kg, respectively; Medistar and Serumwerk, respectively) and transcardially perfused with PBS, followed by 4% paraformaldehyde (PFA, w/v; catalog #1004005, Merck) in PBS. Extracted brains were postfixed at 4°C in 4% PFA (w/v) in PBS for 12 h, embedded in 4% agarose (w/v; catalog #01280, Biomol) in PBS and sliced using a Vibratome (VT1000S, Leica) into 50 or 100 μm free-floating coronal sections.

Mice that underwent calcium imaging experiments were anesthetized with ketamine/xylazine (100 mg/kg and 16 mg/kg, respectively; Medistar and Serumwerk, respectively) and decapitated. The head, together with the GRIN lens implant and baseplate, was fixed at 4°C in 4% PFA (w/v) in PBS for a minimum of 4 d before dissection of the brain. Extracted brains were sliced using a Vibratome (VT1000S, Leica) into 100 μm free-floating coronal sections.

Microscopy

Epifluorescence images were obtained with an upright epifluorescence microscope (Zeiss) with 5×/0.15 or 10×/0.3 objectives (Zeiss). Images were minimally processed with ImageJ software (National Institutes of Health) to adjust for brightness and contrast for optimal representation of the data. A median filter was used to decrease noise.

Quantification and statistical analyses

Extraction of behavioral data for the conditioned place preference assay with food reward. In the conditioned place preference assay, the

←

locations for each animal and expression spread. Locations are shown on schematic coronal section planes with distances (anterior–posterior axis) from bregma. ***G***, PI for the food-paired chamber positive (+ context) during recall after inhibition of CeA neurons during conditioning (Mann–Whitney *U* test, for PKCδ group comparison: $U = 1$, $p = 0.0021$; for Sst group comparison: $U = 29$, $p = 0.7927$). ***H***, ***I***, PI for the food-paired chamber before and after conditioning for CeA^{Sst} (***H***) and $CeA^{PKC\delta}$ neuron-inhibited animals (***I***) and respective control mice. ***J***, ***K***, Representative heat maps of the behavior of individual PKCδ-eNpHR3.0 and PKCδ-mCherry mice during recall. Green represents the minimum and purple the maximum per-pixel frequency. ***L***, Number of visits to the food zone during recall (2-tailed unpaired *t* test, for PKCδ group comparison: $t_{(13)} = 0.5618$, $p = 0.5838$; for Sst group comparison: $t_{(14)} = 1.772$, $p = 0.0982$). ***M***, PI for the food zone during recall (Mann–Whitney *U* test, for PKCδ group comparison: $U = 10.5$, $p = 0.0489$; for Sst group comparison: $U = 14$, $p = 0.0650$). ***N***, Velocity during recall (2-tailed unpaired *t* test, for PKCδ group comparison: $t_{(13)} = 0.6142$, $p = 0.5497$; for Sst group comparison: $t_{(14)} = 0.7520$, $p = 0.4645$). ***O***, Cumulative amount of food eaten during the four training days (2-tailed unpaired *t* test, for PKCδ group comparison: $t_{(13)} = 0.3398$, $p = 0.7394$; for Sst group comparison: $t_{(14)} = 1.141$, $p = 0.2730$). ***P***, ***Q***, Representative traces (in red) of the behavior of PKCδ-eNpHR3.0 (***P*$_1$**), PKCδ-mCherry (***P*$_2$**), Sst-eNpHR3.0 (***Q*$_1$**), and Sst-mCherry mice (***Q*$_2$**) during the open-field task. The yellow square represents the center. ***R***, Cumulative duration in center during the open-field task (Mann–Whitney *U* test, for PKCδ group comparison: $U = 33$, $p = 0.8096$; for Sst group comparison: $U = 25.5$, $p = 0.8168$). ***S***, Number of visits to the center during the open-field task (2-tailed unpaired *t* test, for PKCδ group comparison: $t_{(15)} = 1.033$, $p = 0.3181$; for Sst group comparison: $t_{(13)} = 0.3481$, $p = 0.7334$). ***T***, Velocity during the open-field task (2-tailed unpaired *t* test, for PKCδ group comparison: $t_{(15)} = 0.6166$, $p = 0.5467$; for Sst group comparison: $t_{(13)} = 1.348$, $p = 0.2006$; ***G–O***, $n = 8$ PKCδ-eNpHR3.0 and 7 PKCδ-mCherry mice, $n = 8$ Sst-eNpHR3.0, and $n = 8$ Sst-mCherry mice; ***P–T***, $n = 9$ PKCδ-eNpHR3.0 and 8 PKCδ mCherry mice, $n = 7$ Sst-eNpHR3.0, and $n = 8$ Sst-mCherry mice). Bar graphs show mean ± SEM, and each dot is the quantification of a single animal; ns, Not significant, *$p < 0.05$, **$p <$ 0. 01. CeC/L, Central capsular and central lateral amygdala; BLa, basolateral amygdala; CeM, central medial amygdala.

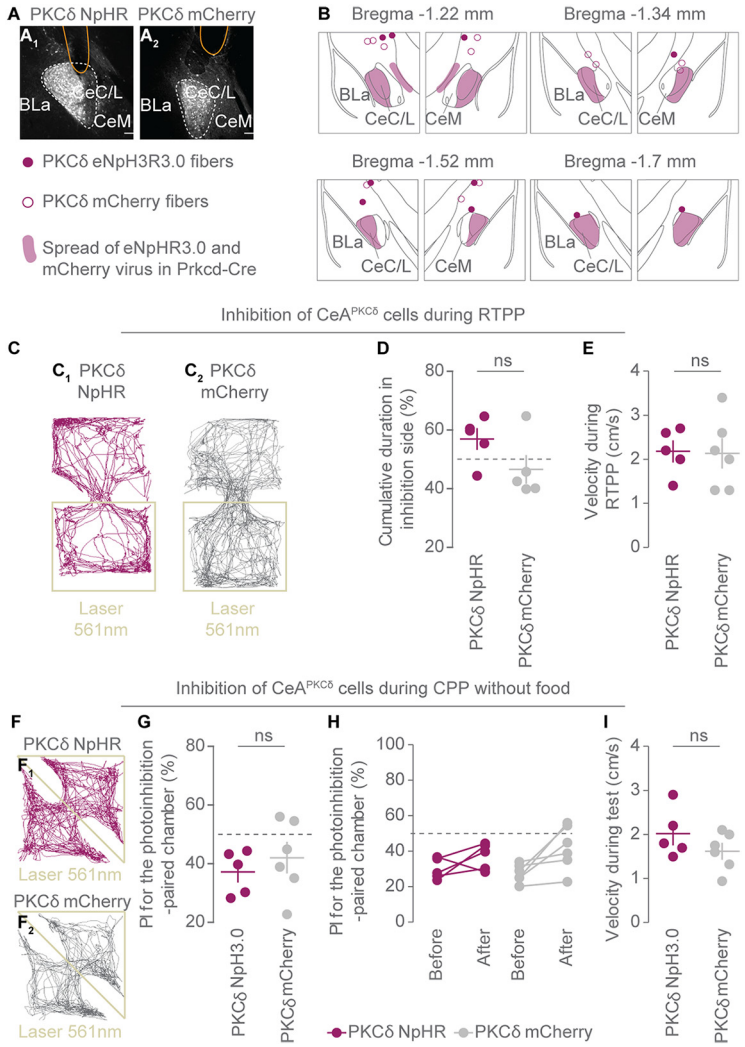

Figure 2. Inhibition of CeA$^{PKC\delta}$ neurons does not result in assigning a rewarding or an aversive signal. ***A***, Representative epifluorescent images of Prkcd-Cre mice injected in the CeL with an AAV-DIO-eNPHR3.0-mCherry (***A$_1$***) or AAV-DIO-mCherry (***A$_2$***) and showing the location of the optic fiber tract (in yellow). Scale bars: 100 µm. ***B***, Approximate optic fiber locations for each animal and expression spread. Locations are shown on schematic coronal section planes with distances (anterior–posterior axis) from bregma. ***C***, Representative traces of the behavior of PKCδ-eNpHR3.0 (***C$_1$***) and PKCδ-mCherry (***C$_2$***) during the RTPP task. ***D***, Cumulative duration in the photoinhibition-paired side during the RTPP assay (Mann–Whitney *U* test, $U = 6.0$, $p = 0.2222$). ***E***, Velocity during RTPP (2-tailed unpaired *t* test: $t_{(9)} = 0.1112$, $p = 0.9139$). ***F***, Representative traces of the behavior of PKCδ-eNpHR3.0 (***F$_1$***) and PKCδ-mCherry (***F$_2$***) during the CPP without food task. ***G***, PI for the photoinhibition-paired chamber during recall after inhibition of CeA neurons during conditioning and in the absence of food (Mann–Whitney *U* test: $U = 11$, $p = 0.5368$). ***H***, PI for the photoinhibition-paired chamber before and after conditioning for CeA$^{PKC\delta}$ neuron-inhibited animals and respective control mice ($n = 5$ PKCδ-eNpHR3.0 and 6 PKCδ-mCherry). ***I***, Velocity during CPP without food (2-tailed unpaired *t* test: $t_{(9)} = 1.350$, $p = 0.2099$). Bar graphs show mean ± SEM, and each dot is the quantification of a single animal. ns, Not significant; CeC/L, central capsular and central lateral amygdala; BLa, basolateral amygdala; CeM, central medial amygdala.

animal location was recorded at 15 Hz using a webcam (Logitech) suspended above the arena, and velocity as well as the preference index and number of entries to the positive context and the food zone were automatically analyzed by EthoVision XT 14 software (Noldus).

For analysis of the calcium recordings, we could not directly score feeding bouts as we only used a camera that was suspended above the arena. Therefore, we manually scored the amount of time when the animals were on top of the food and chose a criteria of 2.5 s as a minimum time to define a feeding bout.

Extraction of behavioral data for the open-field task. Animal location was recorded at 15 Hz using a webcam (Logitech) suspended above the arena, and the number of entries to the center of the arena (20 cm × 20 cm square), cumulative duration in center, and velocity were assessed with EthoVision XT 14 software (Noldus).

Extraction of behavioral data for the RTPP. Animal location was recorded at 15 Hz using a webcam (Logitech) suspended above the arena, and the location of the animal and the velocity were assessed using EthoVision XT 14 (Noldus). Cumulative duration in the photoinhibition-paired chamber was averaged across two sessions.

Extraction of behavioral data for the conditioned place preference assay without food reward. Animal location was recorded at 15 Hz using a webcam (Logitech) suspended above the arena, and the preference index for the photoinhibition-paired chamber and the velocity were assessed using EthoVision XT 14 (Noldus).

Extraction of ΔF/F and temporal registration with behavioral data. For imaging data processing and analysis, all videos recorded from one imaging session were combined into a single image stack using the Inscopix data processing software (version 1.3.0, Inscopix) and saved in a tag image file format (TIFF). TIFF files were then processed using the miniscope 1-photon imaging signal extraction pipeline (MIN1PIPE; Lu et al., 2018), which returns fully processed region-of-interest (ROI) components with spatial footprints and temporal calcium traces as outputs. Briefly, the data go through different steps of neural enhancing, hierarchical movement correction, and neural signal extraction that combine a first seeds-cleansing step followed by a simplified spatiotemporal CNMF (constrained nonnegative matrix factorization). Behavioral data were finally temporally aligned to the calcium traces using linear interpolation and unix time stamps as references for both datasets.

Longitudinal registration of ROIs . ROIs from several recording sessions were longitudinally registered using CellReg MATLAB GUI (Sheintuch et al., 2017; https://github.com/zivlab/CellReg). In brief, the roifn output variable from the MIN1PIPE that contains the processed vectorized ROI footprints for each session was transformed in MATLAB using the following:

roi_use = permute(reshape(roifn, pixh, pixw, n), [3, 1, 2]), where *n* is the number of ROIs.

Transformed ROI footprints were then registered using CellReg and the following parameters: alignment type: translations and rotations (maximum rotation in degrees: 30). A maximal distance of 12 μm was used to compute the probabilistic model. The initial and final cell registrations were performed using spatial correlation models. The resulting cell_to_index_map file was used to identify identical ROIs between different days and calculate the total number of recorded cells per animal and the number of overlapping neurons during the whole recording session.

Regressors and correlation analyses. Regressors were built as previously described (Miri et al., 2011). For this, the behavior of each mouse in the positive context, food zone or on top of the food (square-wave datasets) was convolved with a kernel with an exponential decay based on the measured half-decay time for GCaMP6s (~0.150 s; Chen et al., 2013). The resulting predicted calcium traces were then used to compute Pearson's correlation coefficients with the corresponding calcium traces. To classify neurons as neurons encoding appetitive context, food

responsive cells, or unresponsive in positive context, we examined which coefficients rise above or below chance by correlating our fluorescent traces to 1000 random regressors that were constructed after randomly shuffling the real behavioral dataset by bouts of 20 s. We required a threshold of 1.96 deviation from the Se of the random coefficients mean (corresponding to the 95% confidence interval) to assign a cell to a particular functional group.

Classification of neurons preferentially active in the positive context. To quantify which neurons were preferentially active in the positive context compared with the neutral one during conditioning, ΔF/F transients were *z*-scored at each time point using the following formula: $F(t)$–Fm)/SD, where $F(t)$ is the ΔF/F value at a time *t*, and Fm and SD are the mean and SD of the baseline calculated from the time point when the animals were in the neutral context. An average of the single *z*-scored time points was then calculated for when the animal was located in the positive context. Neurons were considered to be preferentially active in the positive context when the averaged *z*-scored value exceeded the 1.96 threshold (corresponding to the 95% confidence interval).

Decoding of positive and neutral context locations. To decode the location of the mice in the positive or neutral context during recall, we used a logistic regression classifier. For decoder training and testing, we used neuronal Ca^{2+} signals expressed as ΔF/F. For each animal, classifiers were trained on 70% of the data during recall and tested on the remaining 30%. We computed the prediction score as the average of correct predictions over a 10-fold cross-validation procedure. Correct predictions were defined as the ratio of TP/(TP + FP + FN) where TP is the number of true positives, FP the number of false positives, and FN the number of false negatives.

To evaluate the statistical significance of decoding performance, we trained logistic regression decoders on temporally shuffled behavioral data. For this, behavioral data were split into 7 s bouts and randomly shuffled. This was repeated five times. The shuffled prediction score was defined as the average of correct predictions of these five repetitions.

Alignment of calcium responses to positive and neutral context entries. ΔF/F transients were *z*-scored with the baseline calculated from time points when the animals were in the neutral context for alignment to positive context entries, or with the baseline calculated from time points when the animals were in the positive context (for alignment to neutral context entries; see formula above, Classification of neurons preferentially active in the positive context). We omitted short bouts whose duration was below 2.5 s to exclude epochs when the animals were only shortly going in and of the corridor space without fully entering the context. The *z*-scored calcium responses of single neurons to context entry were then averaged in a time window from 3 s before transition to 4.5 s after. Cells were finally sorted in a descending order based on their activity response on entry in the positive context.

Heat maps of the spatial Ca^{2+} activity. To plot a heat map of the average spatial activity of one selected cell we used the raw ΔF/F data. The total activity in a specific *x-y* location was normalized to the total time the animal spent in that location. The x-y data were discretized in 50×50 pixels.

Statistical analysis. No statistical methods were used to predetermine sample sizes. The numbers of samples in each group were based on those used in previously published studies. Behavioral experiments were conducted by an investigator with knowledge of the animal genotype and treatment. For behavioral and *in vivo* imaging experiments, behavioral-tracking software and custom-written Python scripts were used to obtain and analyze the data in an automated and unbiased manner. Statistical analyses were performed with Prism 5 (GraphPad), and all statistics are provided in the figure legends. For individual comparisons of normally distributed data, *t* tests were used. When normality was not assumed, Mann–Whitney *U* test and Wilcoxon signed-rank test (for paired observations) were performed for individual comparisons. A one-way repeated-measures ANOVA or Friedman's test (as a nonparametric equivalent) was used for within-subject comparisons followed by Bonferroni *post hoc* analysis or Dunn's multiple-comparisons test. After the conclusion of experiments, virus-expression, optic-fiber, and GRIN-lens placement were verified. Mice with null virus expression as well as mice in which both optical fibers were wrongly located or at least >500 μm above the CeA were excluded from analysis.

Data availability

The datasets supporting the current study are available from the corresponding author on request. This study used custom-built Python 3.0 programmed scripts, which are also available from the corresponding author on request.

Results

Inhibition of $CeA^{PKC\delta}$ neurons impairs contextual appetitive conditioning

To assess the contributions of CeA subpopulations to the acquisition of contextual appetitive memories, we trained mice in conditioned place preference experiments to associate one chamber (positive context) of a two-chamber arena with a food reward (Fig. 1*A*). Following conditioning, we measured the amount of time the mice spent in the positive context in the absence of food as a readout for contextual appetitive learning. Typically, WT mice learned the task well, spending on average of 71.9 ± 7.2% of their time in the positive context (Fig. 1*B*).

We focused on $CeA^{PKC\delta}$ and CeA^{Sst} neurons because they represent two nonoverlapping populations of central amygdala cells, representing the majority of all neurons in this region (Kim et al., 2017), and, when studied in parallel, mediate antagonizing behaviors (Kim et al., 2017; Wilson et al., 2019; Kargl et al., 2020). We optogenetically inhibited either $CeA^{PKC\delta}$ or CeA^{Sst} neurons during all conditioning sessions (in both the positive and the neutral contexts) by transducing the CeAs of *Prkcd-Cre* or *Sst-Cre* animals with Cre-dependent halorhodopsin-expressing virus (eNpHR3.0-mCherry) and placing optic fibers bilaterally above the CeA (Fig. 1*C–F*). Control mice expressing mCherry behaved similarly to WT mice, although their PI after learning was slightly lower (61.4 ± 2.9% for PKCδ mCherry, and 69 ± 5.1% for Sst mCherry mice; Fig. 1*G–I*). Silencing of CeA^{Sst} neurons did not alter behavior (Fig. 1*G*, *H*). In contrast, $CeA^{PKC\delta}$ neuron-inhibited mice showed poor learning performance, lacking a preference for the positive context during recall (Fig. 1*G*,*I*). In addition, $CeA^{PKC\delta}$, but not CeA^{Sst}, neuron-inhibited animals spent significantly less time in the food zone of the positive context (Fig. 1*J–L*), although they visited it with the same frequency as control mice (Fig. 1*M*).

Several other parameters that may have influenced the outcome of this learning paradigm were found to be similar between the experimental groups, including velocity during recall (Fig. 1*N*), the amount of food eaten during training (Fig. 1*O*), and the degree of anxiety as measured by duration and entries to the center, as well as velocity, in an open-field task (Fig. 1*P–T*).

We further controlled whether inhibition of $CeA^{PKC\delta}$ neuron activity could lead to an assignment of negative or positive valence to both contexts in the absence of food, which could have interfered with the contextual appetitive conditioning. In a real-time place preference assay (RTPP), we found that $CeA^{PKC\delta}$ neuron-inhibited mice exhibited neither a preference nor an aversion for the photoinhibition-paired chamber (Fig. 2*A–E*). We then performed similar conditioned place preference experiments as described in Figure 1*A* but in the absence of a food reward while photoinhibiting $CeA^{PKC\delta}$ cells in one chamber over 4 conditioning days. When we tested the preference of the animals for the photoinhibition-paired chamber, we found that inhibition of $CeA^{PKC\delta}$ neurons alone without food did not produce a conditioned place preference nor an aversion for the photoinhibition-paired chamber (Fig.

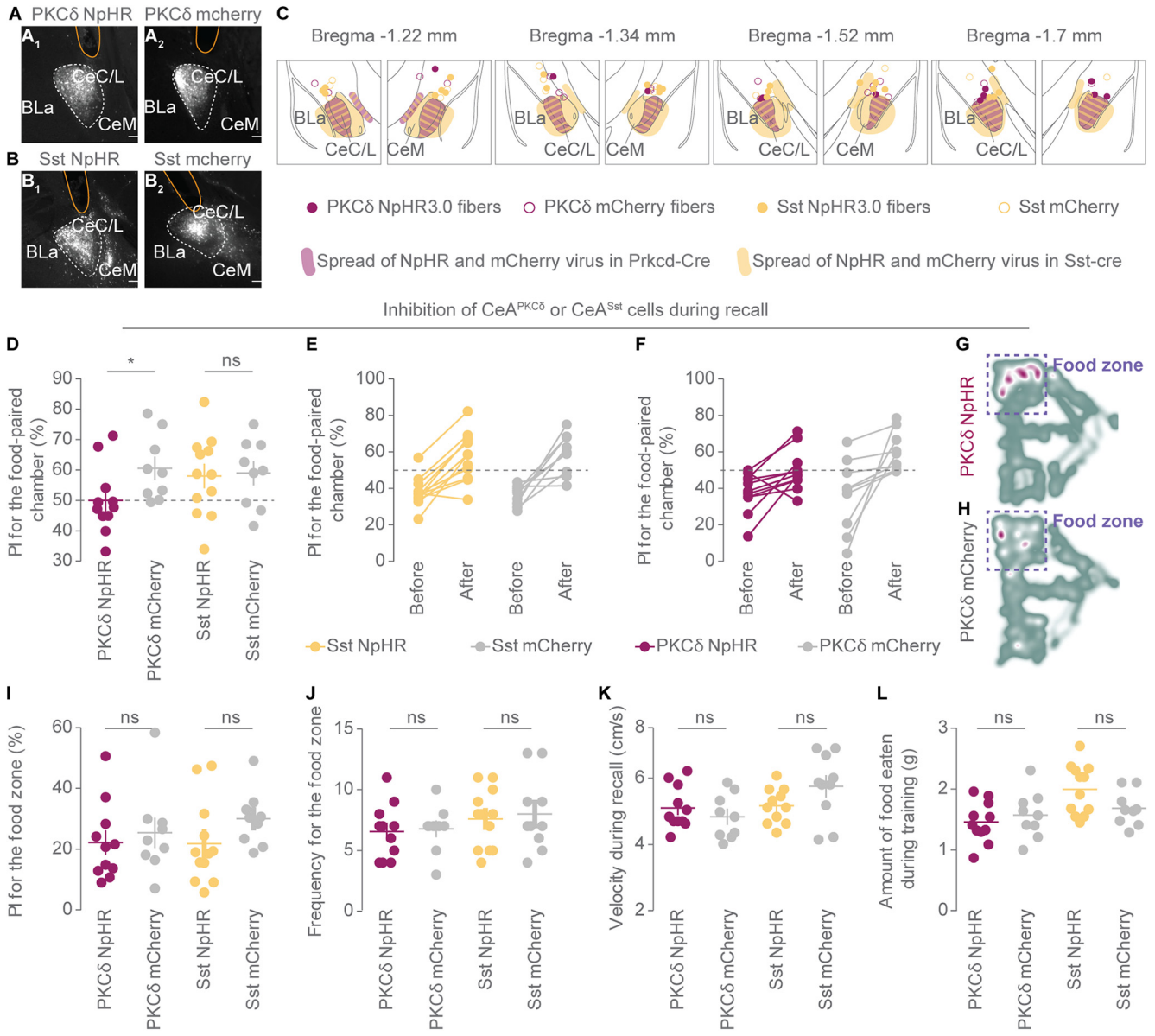

Figure 3. Inhibition of CeA$^{PKC\delta}$ neurons during recall impairs contextual appetitive conditioning. ***A***, ***B***, Representative epifluorescent images of Prkcd-Cre (***A***) and Sst-Cre mice (***B***) injected in the CeL with an AAV-DIO-eNPHR3.0-mCherry (***A$_1$***, ***B$_1$***) or AAV-DIO-mCherry (***A$_2$***, ***B$_2$***) and showing the location of the optic fiber tract (in yellow). Scale bars: 100 µm. ***C***, Approximate optic fiber locations for each animal and expression spread. Locations are shown on schematic coronal section planes with distances (anterior–posterior axis) from bregma. ***D***, PI for the food-paired chamber (+ context) during recall while inhibiting CeA neurons during recall only (Mann–Whitney *U* test, for PKCδ group comparison: $U = 19.5$, $p = 0.0250$; for Sst group comparison: $U = 49$, $p = 0.7491$). ***E***, ***F***, PI for the positive context before and after conditioning for CeA^{Sst} (***E***), CeA$^{PKC\delta}$ neuron-inhibited animals (***F***), and respective control mice. ***G***, ***H***, Representative heat maps of the behavior of individual PKCδ-eNpHR3.0 and PKCδ-mCherry mice during recall. Green represents the minimum and purple the maximum per-pixel frequency. ***I***, PI for the food zone during recall (Mann–Whitney *U test*, for PKCδ group comparison: $U = 40.0$, $p = 0.4941$; for Sst group comparison: $U = 27$, $p = 0.0597$). ***J***, Number of visits to the food zone during recall (2-tailed unpaired *t* test, for PKCδ group comparison: $t_{(18)} = 0.2447$, $p = 0.8094$; for Sst group comparison: $t_{(20)} = 0.3566$, $p = 0.7251$). ***K***, Velocity during recall (2-tailed unpaired *t* test, for PKCδ group comparison: $t_{(18)} = 0.8922$, $p = 0.3840$; for Sst group comparison: $t_{(19)} = 1.707$, $p = 0.1041$). ***L***, Cumulative amount of food eaten during the 4 training days (2-tailed unpaired *t* test, for PKCδ group comparison: $t_{(18)} = 0.7204$, $p = 0.4806$; for Sst group comparison: $t_{(14)} = 0.7520$, $p = 0.0686$; $n = 11$ PKCδ-eNpHR3.0 and 9 PKCδ-mCherry mice, $n = 12$ Sst-eNpHR3.0, and $n = 9$ Sst-mCherry mice). Bar graphs show mean ± SEM, and each dot is the quantification of a single animal. ns, Not significant, $^*p < 0.05$. CeC/L, Central capsular and central lateral amygdala; BLa, basolateral amygdala; CeM, central medial amygdala.

2*A*,*B*, *F*–*I*) indicating that inhibition of activity of these cells alone did not participate in assigning a rewarding or an aversive signal.

We next examined the roles of these two populations during memory retrieval or expression. We used the same tools as before (Fig. 1*C*), except this time we selectively inhibited CeA$^{PKC\delta}$ or CeA^{Sst} cells only during the recall phase. Similar to inhibition of CeA neurons during the conditioning phase, we found that inactivation of CeA$^{PKC\delta}$, but not CeA^{Sst}, cells significantly decreased the preference of the animals for the positive context compared with control mice (Fig. 3*A*–*F*), although the time spent in the food zone (Fig. 3*G*–*I*), as well as the frequency of visits (Fig. 3*J*), remained unchanged. Control parameters such as the velocity during recall (Fig. 3*K*) and amount of food eaten during training (Fig. 3*L*) were similar between groups. Overall, these results suggest that CeA$^{PKC\delta}$ neurons may play a role in forming and retrieving associations between contextual cues and food availability.

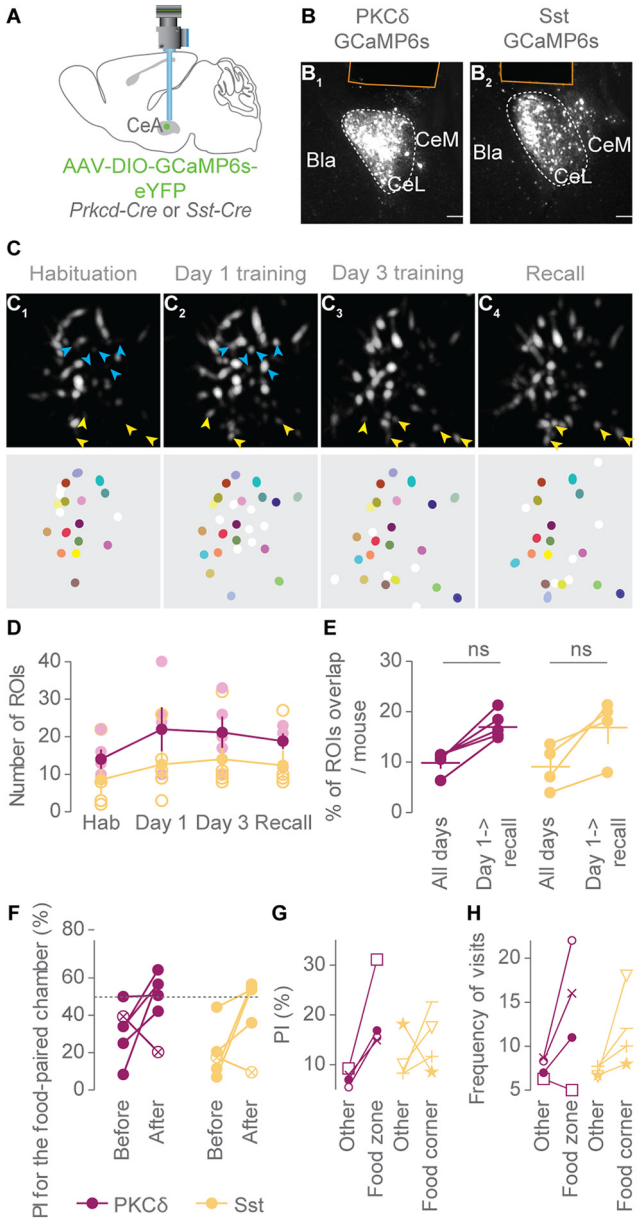

Figure 4. *In vivo* calcium imaging of CeA$^{PKC\delta}$ and CeA^{SST} neurons ***A***, Calcium imaging of CeA$^{PKC\delta}$ and CeA^{Sst} neurons via miniscope in freely moving mice. ***B***, Representative epifluorescent images of Prkcd-Cre (***B$_1$***) and Sst-Cre mice (***B$_2$***) injected in the CeL with an AAV5-Syn. Flex.GCaMP6s and showing the location of the GRIN lens tract (in yellow). Scale bars: 100 µm. ***C***, Maximum projection images of PKCδ+ GCaMP6s-expressing neurons from a representative mouse recorded during habituation (***C$_1$***), first (***C$_2$***) and third (***C$_3$***) days of training, as well as recall (***C$_4$***). Bottom, Corresponding ROIs are depicted. ROIs identified over consecutive sessions are shown in identical color. ROIs detected only in one session are shown in white. Blue arrowheads indicate neurons that appeared for the first time on day 1 of conditioning. Yellow arrowheads indicate neurons that are common between at least 2 of 3 d of conditioning and recall and are not visible on habituation. ***D***, Numbers of detected ROIs during all four sessions (1-way repeated-measures ANOVA, for PKCδ group comparisons: time point, $F_{(3,4)} = 2.16$, $p = 0.1458$; for Sst group comparisons: time point, $F_{(3,4)} = 3.98$, $p = 0.0351$). ***E***, Percentage of ROIs per Prkcd-Cre and Sst-Cre mice that overlapped in all four recording sessions or from day 1 of conditioning to recall (Wilcoxon signed-rank test, for PKCδ comparison: $p = 0.125$; for Sst group comparison: $p = 0.25$). ***F***, PI for the positive context before and after conditioning for both PKCδ- and Sst-GCaMP6s recorded mice. Data points shown as crossed circles represent mice that did not show an increase in learning after conditioning. ***G***, Cumulative duration in food zone compared with the averaged cumulative duration in the other three corners for the 4 PKCδ- and 4 Sst-GCaMP6s mice that are considered to have learned the task (***F***). Similar symbols represent the same mice. ***H***, Frequency of visits to the food zone compared with the averaged frequency of visits in the other three corners for the 4 PKCδ- and 4 Sst-GCaMP6s recorded mice that are considered to have learned the task (***F***). Similar symbols represent the same mice ($n = 5$ PKCδ-GCaMP6s and $n = 5$ Sst-GCaMP6s recorded animals). Bar graphs show mean ± SEM, each dot is the quantification of a single animal. ns, Not significant.

In vivo recordings of CeA$^{PKC\delta}$ and CeA^{Sst} neuron activity during appetitive conditioning

To understand how CeA$^{PKC\delta}$ and CeA^{Sst} neuron activity differentially contributes to this behavior, we expressed the GCaMP6s indicator in the CeA of PKCδ+ and Sst+ cells and recorded the dynamics of fluorescent signals using a miniscope during all phases of the task (Fig. 4*A–C*). Mice were subjected to the same behavioral task, and at the end of the recall, a food pellet was added to the positive context to make sure that we could functionally tag food responsive neurons.

We recorded the activities of 24–61 cells per mouse (202 cells total) in five Prkcd-cre mice and 14–60 cells per mouse (149 cells total) in five Sst-cre animals (Fig. 4*D*). The numbers of active cells during training and recall were higher as compared with habituation day in both groups. Longer imaging time during training and especially recall may account for this difference. Alternatively, investigation and consumption of food may have recruited new sets of neurons (Fig. 4*C*,*D*). Using an ROI alignment method (Sheintuch et al., 2017), we registered cell identities across imaging sessions. We found ~10% of cells in common for all 4 recording days (Fig. 4*E*). When excluding the habituation day, the number of common cells increased to ~17% in both Cre lines (Fig. 4*E*), suggesting that neurons recorded during conditioning and recall may be functionally more similar than the ones initially active during habituation. Of 10 recorded mice, three per genotype showed a PI ≥50% during recall, which is lower than observed before (Fig. 4*F*). It is possible that the weight of the miniscope rendered movements more laborious and decreased performance. Nonetheless, eight animals of 10 increased their preference for the positive context after conditioning (Fig. 4*F*), spending on average 2.1 times longer in the food zone and visiting it 1.7 times more often compared with the other three corners of the arena (Fig. 4*G*,*H*). Together, these are good indications that those eight animals learned the task.

Central amygdala encoding of pavlovian appetitive learning

We tested the Hebbian model of appetitive conditioning (Hebb, 1949; Brown et al., 1990; Sejnowski, 1999) by investigating whether the positive context, which represents multisensory information, could serve as a general predictor of food availability after learning. Or, in other words, could CeA neurons that fire during food intake acquire a specific response to the positive context after learning?

Taking into account only the data of the eight mice that learned the task (Fig. 4*F–H*), we convolved the positive context signal with the kinetics of the calcium indicator to create a regressor and correlated the activity of each CeA cell with the corresponding regressor across time (Miri et al., 2011). An example trace of a positive context regressor is shown at the bottom of Figure 5*K*. We found that during habituation, the activities of all neurons showed little correlation to the positive context. Instead, during recall, the activities of both populations shifted toward positive correlations (Fig. 5*A*,*B*), suggesting that the representations of the positive chamber by CeA$^{PKC\delta}$ and CeA^{Sst} neurons were transformed after learning.

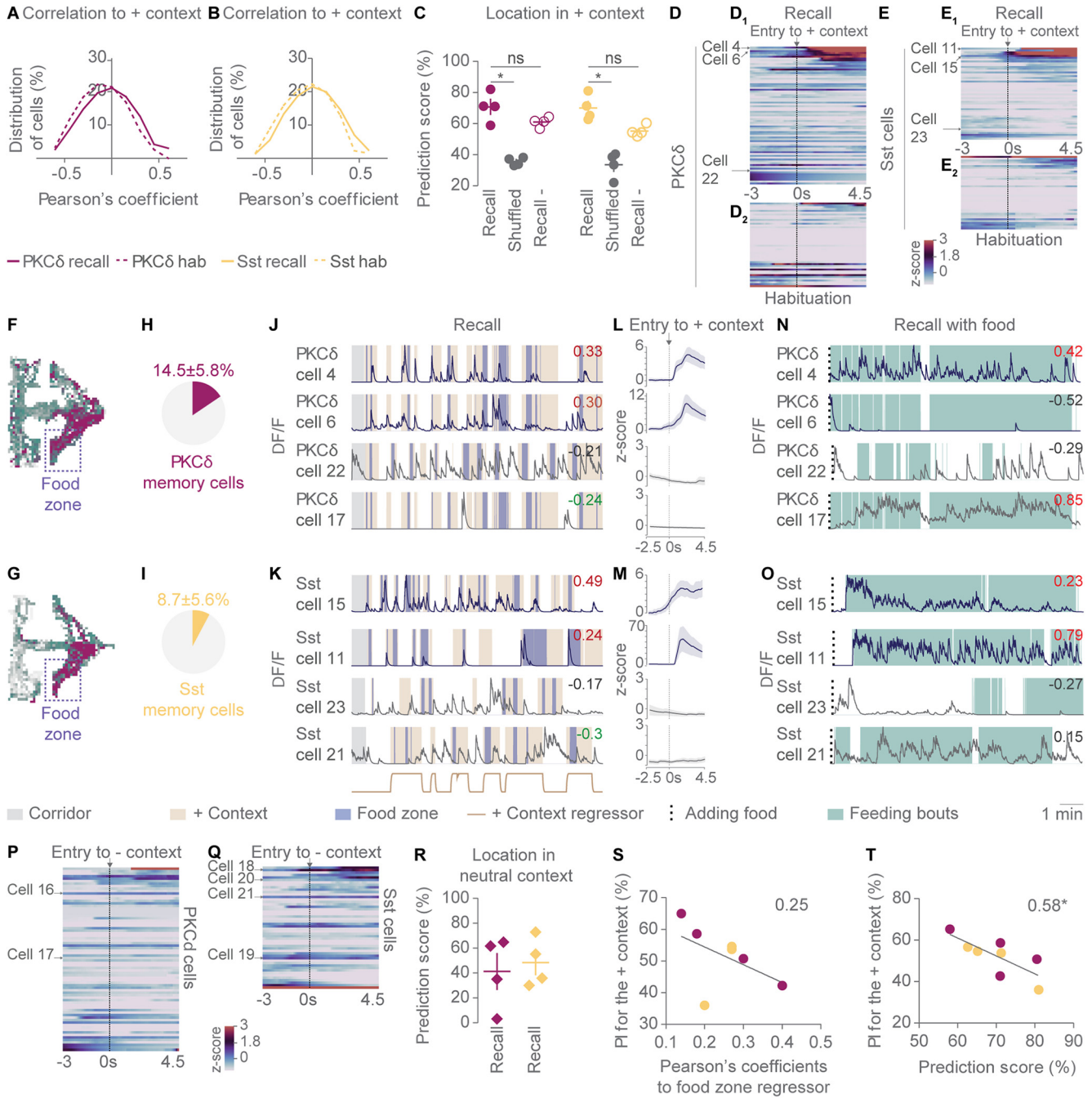

Figure 5. Central amygdala encoding of pavlovian appetitive learning. ***A***, ***B***, Frequency distribution of Pearson's correlation to the positive context regressor in PKCδ (***A***) and SST (***B***) calcium recorded neurons during habituation and recall. ***C***, Prediction scores of the locations of Prkcd-Cre (purple) and Sst-Cre (yellow) calcium recorded animals in the positive context during recall, after temporally shuffling of behavioral data (shuffled) and after excluding four neurons per animal that exhibited the highest correlation value to the positive context regressor (recall −; Friedman test, for PKCδ group comparisons: $F = 9.9$, $p = 0.0062$ with Dunn's multiple-comparisons test; for Sst group comparisons: $F = 9.3$, $p = 0.0115$ with Dunn's multiple-comparisons test, *$p < 0.05$). ***D***, ***E***, Heat maps of average *z*-scored calcium responses of PKCδ (***D***) and SST (***E***) recorded neurons following entry to the positive context (at 0 s) during recall (***D$_1$***, ***E$_1$***) and during habituation (***D$_2$***, ***E$_2$***). Cells were sorted in descending order based on their activity response on entry in the + context (entries to the + context varied from 6 to 14 times depending on the mice; $n = 75$ PKCδ + and 50 Sst+ neurons). ***F***, ***G***, Heat maps of the ΔF/F signal across the whole arena for one representative PKCδ (***F***) and Sst (***G***) neuron encoding appetitive context. Green represents the minimum and purple the maximum per-pixel frequency (Extended Data Figure 5-1*A*). ***H***, ***I***, Fraction of CeA neurons encoding appetitive context in Prkcd-cre (***H***) and Sst-cre (***I***) recorded animals during recall. ***J***, ***K***, Representative Ca^{2+} traces (from 7 mice) of PKCδ (***J***) and Sst (***K***) recorded neurons during recall. The trace in beige (***K***, bottom) represents the convolved GCaMP6s regressor for the positive context of cell 21 (Extended Data Figure 5-1*A*). Values indicate the Pearson's coefficients of each cell to its corresponding positive context regressor. Values in green indicate a significant negative correlation. Each ΔF/F trace was normalized to its maximum value. ***L***, ***M***, Average traces of the corresponding PKCδ (***L***) and Sst (***M***) neurons (left) following entry to the positive context (at 0 s). Cells 4, 6, 15, and 11 are four representative neurons encoding the appetitive context after learning. Cells 22 and 23 are nonmemory cells, cells 17 and 21 are neurons whose activity is negatively correlated to the positive context. Shaded areas represent SEM. ***N***, ***O***, Ca^{2+} signals of the corresponding PKCδ (***N***) and Sst (***O***) neurons shown in ***J*** and ***K*** on introduction of a food pellet in the food zone (dotted line) at the end of the place preference assay. Values indicate the Pearson's coefficients of each cell to its corresponding feeding bouts regressor. Values in red indicate a significant correlation. Each ΔF/F trace was normalized to its maximum value. ***P***, ***Q***, Heat map of averaged *z*-scored calcium responses of PKCδ (***P***) and SST (***Q***) recorded neurons following entry to the neutral context [negative (−) context at 0 s]. ΔF/F transients were *z*-scored with the baseline calculated from time points when the animals were in the positive context. Cells were sorted in descending order based on their activity response on entry in the negative context ($n = 75$ PKCδ + and 50 Sst+ neurons). ***R***, Prediction scores of the locations of Prkcd-Cre (purple) and Sst-Cre (yellow) calcium recorded animals in the neutral context during recall. ***S***, PI in the positive context on recall day as a

For each mouse, we randomly selected 70% of the data during recall to train a logistic regression classifier and asked whether in the remaining dataset the location of the mice in the positive context could be accurately predicted based on $CeA^{PKC\delta}$ and CeA^{Sst} population activity. In all mice tested, we could reliably decode the position of the animals in the positive chamber (70.7 ± 4.7% for $CeA^{PKC\delta}$ and 70 ± 4.1% for CeA^{Sst} recorded ensembles), whereas performances significantly dropped when the decoder was trained on temporally shuffled behavioral data (Fig. 5*C*), indicating that correct predictions were well above chance. We also found a decreased performance of 10% and 15%, respectively, when the classifier was tested on $CeA^{PKC\delta}$ and CeA^{Sst} population activity that excluded the four most important features (defined here as the neurons showing the highest correlations to the positive context; Fig. 5*C*). This suggests that at least a fraction of both populations encoded essential information about the location of the animal in the positive context. When we aligned the neuronal Ca^{2+} responses of each cell to the onset of the transitions from the neutral to the positive context and averaged the data, we found that a subset of both $CeA^{PKC\delta}$ and CeA^{Sst} neurons was activated on transition to the positive context (Fig. 5*D*,*E*). During habituation, we could not identify a group of neurons whose activity reliably increased on entry in the positive chamber, meaning that encoding of the appetitive context by $CeA^{PKC\delta}$ and CeA^{Sst} neurons arose after conditioning (Fig. 5*D*,*E*). These cells exhibited an area-biased activity that was specifically high when the mouse was in the appetitive context and preferentially within the food corner (Fig. 5*F*,*G*). Cells that displayed a significant correlation toward the positive context regressor accounted for ~14.5% of $CeA^{PKC\delta}$ and 8.7% of CeA^{Sst} recorded cells during recall (Fig. 5*H*,*I*). Neurons encoding appetitive context were found in 4/4 Prkcd-cre analyzed mice and 3/4 analyzed Sst-Cre mice (Extended Data Fig. 5-1*A*). Analysis of the ΔF/F traces revealed different patterns of activity within the positive context. Some neurons fired both on entry to the positive chamber and investigation of the food zone (Fig. 5*J*,*L*, cells 4 and 6, *K*,*M*, cell 15). Some cells were active preferentially within the food zone (Fig. 5*K*,*M*, cell 11). Other nonmemory neurons showed no preference for the positive context nor the food zone (Fig. 5*J*–*M*, cells 22 and 23). At this point, no differences were observed between neurons encoding appetitive context within the PKCδ and Sst populations. Again, using a regressor-based approach, we found that the activities of 60% of $CeA^{PKC\delta}$ and all CeA^{Sst} neurons encoding appetitive context were significantly upregulated during food consumption on the same recall day (Fig. 5*N*–*O*, Extended Data Fig. 5-1*A*), demonstrating that a subset of these cells can be tagged as food responsive.

We also looked at neurons that would be particularly unresponsive in the positive context (i.e., significant negative correlation to the positive context regressor), and identified a total of nine PKCδ+ and seven Sst+ neurons. The activity of these neurons was, however, very weak, as only six of them showed a significantly elevated activity in the neutral context (Fig. 5*J*–*M*, cells 17 and 21, Extended Data Fig. 5-1*B*). None of these six identified neurons nor any other recorded cells showed an increased activity on transition to the neutral context (Fig. 5*P*,*Q*). Additionally, we trained the logistic regression classifier on the presence of the mice in the neutral context while omitting the neurons encoding appetitive context for each animal (Fig. 5*H*,*I*). By doing so, we found that performance of the decoder was low (41.2% ± 14.3% for Prkcd-cre, and 48.4% ± 19.5% for Sst-cre recorded mice; Fig. 5*R*). This is a good indication that there may not be any other neurons (in addition to the neurons encoding appetitive context), whose activity can be used to predict the location of the animal in the neutral context.

We found no correlation between the number of neurons encoding appetitive context and the learning index (data not shown), but this could be an issue inherent to the behavioral task; although the poor learners may associate only the precise location of the food zone with a rewarding outcome, the good learners may associate the whole positive context or even the whole arena with food delivery. In the latter case, neurons encoding appetitive context may already fire when the animal recognizes the whole arena, but we do not have the means to visualize them.

This hypothesis is supported by the fact that neurons encoding appetitive context, whose activity best represented the food zone, were found in mice that showed lower learning indices, demonstrated as a negative correlation between the average correlation of neurons encoding appetitive context to the food zone regressor and the PI of the mice (Fig. 5*S*). Additionally, when we compared the prediction scores of our logistic regression decoder with the PI of the mice, we found that decoding accuracy of the classifier decreased with learning performances (Fig. 5*T*). In other words, the classifier did not manage to find a good representation of the positive context in the neural activity of the best learners. It is therefore possible that mice that learned best generalized the representation of the positive context to the whole arena.

Overall, these results suggest that contextual information associated with the positive context became predictive of food delivery after learning and support a model in which groups of $CeA^{PKC\delta}$ and CeA^{Sst} neurons encode contextual food cues in line with a Hebbian plasticity mechanism.

Differences in calcium activity patterns between $CeA^{PKC\delta}$ and CeA^{SST} neurons

Next, we took a step back and examined the activity profiles of all recorded neurons during conditioning, taking into consideration all five Prkcd-cre and five Sst-cre recorded animals (Fig. 4*F*). On day 1 and day 3 of training, we found that a large fraction of both $CeA^{PKC\delta}$ and CeA^{Sst} neurons strongly increased their activity, specifically when the mice were sequestered in the positive context when the food reward was present (Fig. 6*A*–*D*, cells A to F). These cells accounted for 30.9 ± 10.3% of PKCδ and 31.1 ± 7.3% of Sst recorded ensembles on day 1, and their proportion increased to 41.7 ± 6.7% and 58.3 ± 7.8%, respectively, on day 3 of conditioning (Fig. 6*E*).

For each cell, we calculated Pearson's correlations for their corresponding feeding regressor and accordingly classified neurons as activated by food consumption. Interestingly, we observed that $CeA^{PKC\delta}$ cells did not always fire systematically during each feeding bout (Fig. 6*C*). Conversely, CeA^{Sst} neurons increased their activities at the onset of a feeding bout and more reliably for the following ones (Fig. 6*D*). Supporting these observations, on day 1 and on day 3 of training, CeA^{Sst} neurons showed stronger positive correlation to the feeding regressor

←

function of the averaged value of all Pearson's correlation coefficients to the food zone regressor for all identified neurons encoding appetitive context in a given mouse. Each dot represents a single Prkcd-Cre (purple) or Sst-Cre (yellow) animal. Values shown are R^2. ***T***, Prediction score of the logistic regression classifier as a function of the PI of the animal on recall day. Each dot represents a single Prkcd-Cre (purple) or Sst-Cre (yellow) animal. Values shown are R^2 ($n = 4$ PKCδ- and 4 Sst-GCaMP6s recorded animals). Bar graphs show mean ± SEM, and each dot represents a single animal. ns, Not significant, $^*p < 0.05$.

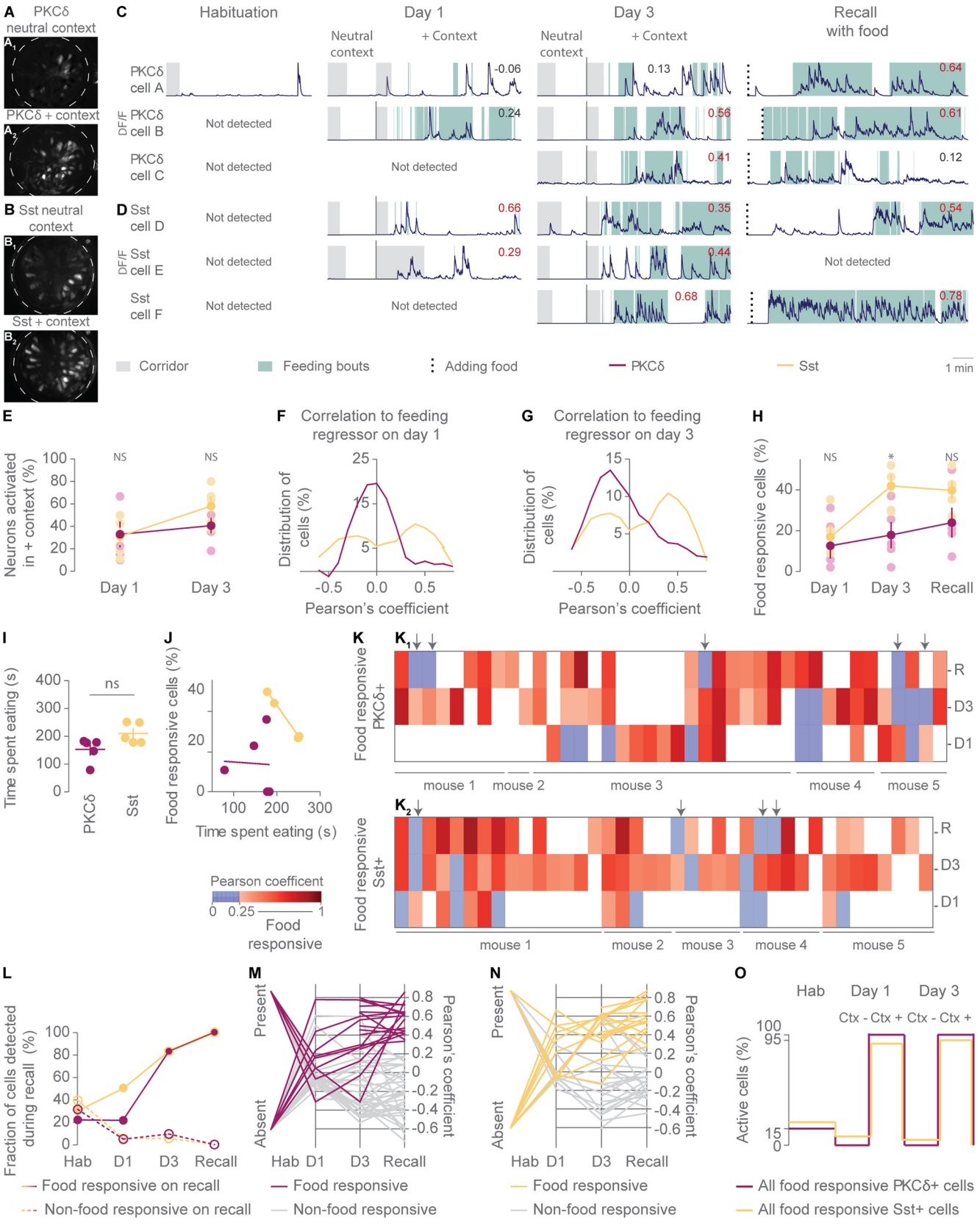

Figure 6. Differences in calcium activity patterns between CeA $^{PKC\delta}$ and CeA^{SST} neurons. ***A***, ***B***, Maximum projection representative images of PKCδ + (***A***) and Sst+ (***B***) GCaMP6s-expressing neurons during day 3 of conditioning in the neutral (***A$_1$*** and ***B$_1$***) and in the positive context (***A$_2$*** and ***B$_2$***). ***C***, ***D***, Representative Ca^{2+} traces (from 6 mice) of PKCδ (***C***) and Sst (***D***) recorded neurons during habituation, day 1, day 3 of conditioning, and recall with food. Colored boxes indicate the location of the mouse in the corridor (gray) or on top of the food (green). The values indicate the Pearson's coefficients of each cell to its corresponding feeding bouts regressor. Values in red indicate a significant correlation. Each ΔF/F trace was normalized to its maximum value. ***E***, Proportion of neurons per mouse that are significantly active in positive (+) context compared with negative (−) context on days 1 and 3 of conditioning. (Mann–Whitney *U* test between PKCδ and Sst on day 1, $U = 11$, $p = 0.8413$; on day 3, $U = 6$, $p = 0.2045$). ***F***, ***G***, Frequency distribution of Pearson's correlations to the feeding bouts regressor in all PKCδ and SST recorded

(Fig. 6*F*,*G*) compared with CeA$^{PKC\delta}$ cells, and the proportion of food responsive cells was higher among the CeA^{Sst} population (Fig. 6*H*). There was no difference in the fraction of PKCδ+ and Sst+ cells active in the positive context during training (Fig. 6*E*), suggesting that the activity of CeA$^{PKC\delta}$ cells may not directly relate to food consumption but rather to the salience of the food reward. This phenotype was not because Pkcd-Cre animals ate less than Sst-Cre, as there was no positive correlation between the amount of time spent eating and the proportion of food responsive cells on day 3 of training (Fig. 6*I*,*J*).

We then tracked neurons over time to see whether they would maintain their food responsiveness over time and, indeed, we found that the majority of cells that showed significant correlation to the feeding regressor on 1 conditioning day conserved their functional tag on the subsequent day (Fig. 6*C*,*D*, cells B, D, E, *K*). Additionally, when tracking PKCδ+ and Sst+ cells that were classified as food responsive on recall, we found that 83% of PKCδ+ and Sst+ were also found food responsive on day 3, and 22% of PKCδ+ and 50% of Sst+ on day 1 (Fig. 6*L*–*N*). In comparison, the majority of nonfood responsive neurons on recall day were classified nonresponsive during the whole task (Fig. 6*L*–*N*). Most food responsive neurons were also significantly active in the positive context compared with the neutral one during all training sessions and were absent during habituation (Fig. 6*C*, cells B and C, *D*, cells D to F, *M*–*O*), together revealing their functional selectivity.

When tracing the origin of the PKCδ and Sst neurons encoding appetitive context (Extended Data Fig. 5-1*A*) we identified two different scenarios: 1) When detected, cells were tagged as food responsive during each step of the whole paradigm, and they were absent during habituation. This scenario includes 60% of the CeA$^{PKC\delta}$ and all CeA^{Sst} neurons encoding appetitive context. 2) Cells were either not food responsive or lost their food responsive tag after conditioning. This includes 40% of the PKCδ neurons encoding appetitive context (found in two mice).

These last findings suggest that during conditioning, CeA^{Sst} cells whose activities show high positive correlation with food intake behavior may be important to link environmental information with the physical properties of the food. In contrast, CeA $^{PKC\delta}$ neurons that are robustly activated on food pellet delivery in the arena, but not reliably on food consumption, might rather form associations between environmental information and the salience of the food reward.

Discussion

Here, we used a conditioned place preference assay allowing us to identify neuronal correlates of appetitive memories as the animal freely moves toward the food. This is noticeably different from classical studies of associative learning that looks at neuronal activity shortly following exposure to a conditioned tone applied by the experimenter (Pare and Quirk, 2017).

We found that two genetically distinct populations of CeA neurons (PKCδ+ and Sst+ neurons), developed specific activity patterns for the chamber associated with the reward. Interestingly, only the activities of CeA$^{PKC\delta}$, but not CeA^{Sst}, cells were required for the formation and early retrieval of a preference for the appetitive context, suggesting that these neurons encode a combination of sensory, reward, and contextual information to support learning that a spatial location predicts food availability.

CeA$^{PKC\delta}$ neurons were previously shown to inhibit appetitive behaviors in response to threats or aversive tastes or in response to satiety (Cai et al., 2014; Kim et al., 2017). Moreover, CeA$^{PKC\delta}$ neurons could be described as broadly aversive because these cells also promote pain-related responses and are linked to the expression of aversive memories (Haubensak et al., 2010; Cui et al., 2017; Wilson et al., 2019). Our findings, instead, suggest that CeA$^{PKC\delta}$ cells may have functions that are more general and relate to a variety of stimuli. This is supported by findings from anesthesia neurons that show an 80% overlap with CeA$^{PKC\delta}$ neurons and attenuate (rather than promote) pain-related behavior (Hua et al., 2020). CeA^{Sst} neurons may also show multidimensional response properties as these neurons relate to appetitive stimuli (Kim et al., 2017; Wilson et al., 2019) but also contribute to the generation of defensive behaviors (Li et al., 2013; Penzo et al., 2015; Yu et al., 2016). Although these findings underscore the notion that molecularly distinct populations represent functionally specialized units, it remains possible that further subdivision of CeA populations using two or three genetic markers will reveal the presence of more specialized cells.

How could CeA$^{PKC\delta}$ neurons mediate learning of contextual food cues? Inhibition of CeA$^{PKC\delta}$ neurons during conditioning did not affect the number of times an animal visited the precise location of the food zone but rather the time spent within this area. This was consistent with our calcium imaging data showing that CeA neurons encoding appetitive context showed a significant increase in activity when the animal was either specifically in the food zone or in the positive context. We interpret these results to mean that the activity of CeA neurons may be relevant to encode a representation of the goal, that is, reward associated with a particular location rather than a representation of compass cues that would help the animal in its search for the food. In the animals that learned best, this memory may initially be linked to the location of the food zone and was then generalized to the

←

neurons during day 1 (***F***) and day 3 (***G***) of conditioning. ***H***, Proportion of neurons per mouse that are food responsive on day 1, day 3 of conditioning, and recall. (Mann–Whitney *U* test between PKCδ and Sst on day 1, $U = 10$, $p = 0.6723$; on day 3, $U = 2$, $p = 0.0362$; and on recall, $U = 4$, $p = 0.0952$). ***I***, Time spent eating during day 3 for PKCδ- and Sst-GCaMP6s recorded mice (2-tailed unpaired *t* test $t_{(8)} = 2.242$, $p = 0.552$). ***J***, Proportion of food responsive PKCδ+ and Sst+ cells as a function of the time spent eating on day 3 of conditioning. ***K***, Heat maps of Pearson's correlations to the feeding bouts regressor for PKCδ (***K*$_1$**) and Sst (***K*$_2$**) neurons that were classified as food responsive on at least one of the recorded days. White represents neurons that were not detected during a recording session. Blue represents no significant correlations, so nonfood responsive cells. Strong correlation values are represented in dark red. Arrows indicate neurons that were classified as food responsive on one day and lost their functional tag on the following one ($n = 40$ PKCδ+ and 39 Sst+ neurons). ***L***, Fraction of food responsive (solid lines) and nonfood responsive cells (dotted lines) detected during recall that are tagged as food responsive on day 3 and 1 of conditioning and present during habituation. ***M***, ***N***, Food responsive PKCδ+ (***M***, purple lines) and Sst+ cells (***N***, yellow lines) as well as nonfood responsive cells (gray lines) detected during recall and traced back to day 3 and day 1 of conditioning and habituation. Each line represents a cell and its correlation value to the feeding regressor on recall, day 3 and day 1 of conditioning, as well as whether it was present or not during habituation. Values above 0.25 represent a significant positive correlation to the feeding regressor ($n = 92$ PKCδ+ and 59 Sst+ neurons). ***O***, Proportion of food responsive PKCδ+ and Sst+ neurons that were active during habituation and that were significantly active in the negative context or the positive context during day 1 and day 3 of conditioning ($n = 40$ PKCδ+ and 39 Sst+ neurons; $n = 5$ PKCδ- and 5 Sst-GCaMP6s recorded animals). Bar graphs show mean ± SEM, and each dot represents a single animal. ns, Not significant,*$p < 0.05$.

positive context and ultimately to the whole arena. Inhibition of $CeA^{PKC\delta}$ neurons during recall also impaired the preference of the animals for the positive context, although the effect was weaker, and the time spent within the food zone was unaffected. This suggests that $CeA^{PKC\delta}$ cells may be involved in the early retrieval of appetitive memories but these memories may be gradually transferred to different brain regions over time (Do Monte et al., 2016).

Although contextual memory traces were observed in subsets of both $CeA^{PKC\delta}$ and CeA^{Sst} neurons, our data uncovered differences between their activity patterns. We found, for instance, that the proportion of neurons active during food intake was significantly higher among the CeA^{Sst} compared with the $CeA^{PKC\delta}$ population. We hypothesize that CeA^{Sst} neurons encoding appetitive context may be essential to link a context or a sensory stimulus with the physical properties of food (e.g., taste, texture, etc.), but preventing this association from forming does not prevent the animals from developing a preference for the food-paired chamber. Conversely, $CeA^{PKC\delta}$ neurons encoding appetitive context may mediate the association of contextual stimuli with the general affective properties of food, a function that has been previously suggested for the CeA (Balleine and Killcross, 2006). Inhibiting the formation of these memories would then impair the ability of an animal to develop a preference for the location of the food reward. It is, however, important to mention here that our conclusions were drawn based on loss-of-function experiments of the entire population but with relevant neuronal activity patterns seen in only a subset of cells. Therefore it is possible that specific inhibition of memory neurons as opposed to whole PKCδ+ or Sst+ populations could lead to a different phenotype. Our data are nonetheless consistent with recent evidence that initially, before learning, $CeA^{PKC\delta}$ neurons are tuned to stimulus salience, but after conditioning, they encode valence discrimination to select the appropriate defensive or appetitive responses (Kargl et al., 2020). Furthermore, $CeA^{PKC\delta}$ neurons seem to be part of a bottom-up network that is necessary to relay reinforcement signals to higher order areas such as the insula cortex (Kargl et al., 2020) and the lateral amygdala (Yu et al., 2017), which ultimately feed back to the CeA to drive associative learning.

In conclusion, our work reports specific activity patterns of CeA neurons that resemble contextual memory traces to appetitive stimuli. We propose that salience coding in PKCδ+ cells is integrated with sensory representations of the environment through pavlovian learning mechanisms to drive correct behavioral choices during foraging.

References

Balleine BW, Killcross S (2006) Parallel incentive processing: an integrated view of amygdala function. Trends Neurosci 29:272–279.

Brown TH, Kairiss EW, Keenan CL (1990) Hebbian synapses: biophysical mechanisms and algorithms. Annu Rev Neurosci 13:475–511.

Cai H, Haubensak W, Anthony TE, Anderson DJ (2014) Central amygdala PKC-δ+ neurons mediate the influence of multiple anorexigenic signals. Nat Neurosci 17:1240–1248.

Chen TW, Wardill TJ, Sun Y, Pulver SR, Renninger SL, Baohan A, Schreiter ER, Kerr RA, Orger MB, Jayaraman V, Looger LL, Svoboda K, Kim DS (2013) Ultrasensitive fluorescent proteins for imaging neuronal activity. Nature 499:295–300.

Ciocchi S, Herry C, Grenier F, Wolff SBE, Letzkus JJ, Vlachos I, Ehrlich I, Sprengel R, Deisseroth K, Stadler MB, Müller C, Lüthi A (2010) Encoding of conditioned fear in central amygdala inhibitory circuits. Nature 468:277–282.

Corbit LH, Balleine BW (2005) Double dissociation of basolateral and central amygdala lesions on the general and outcome-specific forms of pavlovian-instrumental transfer. J Neurosci 25:962–970.

Cui Y, Lv G, Jin S, Peng J, Yuan J, He X, Gong H, Xu F, Xu T, Li H (2017) A central amygdala-substantia innominata neural circuitry encodes aversive reinforcement signals. Cell Rep 21:1770–1782.

Do Monte F, Quirk G, Li B, Penzo M (2016) Retrieving fear memories, as time goes by.... Mol Psychiatry 21:1027–1036.

Douglass AM, Kucukdereli H, Ponserre M, Markovic M, Gründemann J, Strobel C, Alcala Morales PL, Conzelmann KK, Lüthi A, Klein R (2017) Central amygdala circuits modulate food consumption through a positive-valence mechanism. Nat Neurosci 20:1384–1394.

Ehrlich I, Humeau Y, Grenier F, Ciocchi S, Herry C, Lüthi A (2009) Amygdala inhibitory circuits and the control of fear memory. Neuron 62:757–771.

Fadok JP, Markovic M, Tovote P, Lüthi A (2018) New perspectives on central amygdala function. Curr Opin Neurobiol 49:141–147.

Gallagher M, Graham PW, Holland PC, Graham WP, Holland PC, Graham PW (1990) The amygdala central nucleus and appetitive pavlovian conditioning: lesions impair one class of conditioned behavior. J Neurosci 10:1906–1911.

Han JS, McMahan RW, Holland P, Gallagher M (1997) The role of an amygdalo-nigrostriatal pathway in associative learning. J Neurosci 17:3913–3919.

Han JS, Holland PC, Gallagher M (1999) Disconnection of the amygdala central nucleus and substantia innominata/nucleus basalis disrupts increments in conditioned stimulus processing in rats. Behav Neurosci 113:143–151.

Haubensak W, Kunwar PS, Cai H, Ciocchi S, Wall NR, Ponnusamy R, Biag J, Dong HW, Deisseroth K, Callaway EM, Fanselow MS, Lüthi A, Anderson DJ (2010) Genetic dissection of an amygdala microcircuit that gates conditioned fear. Nature 468:270–276.

Hebb DO (1949) The organization of behavior. New York: Wiley.

Herry C, Johansen JP (2014) Encoding of fear learning and memory in distributed neuronal circuits. Nat Neurosci 17:1644–1654.

Hua T, Chen B, Lu D, Sakurai K, Zhao S, Han BX, Kim J, Yin L, Chen Y, Lu J, Wang F (2020) General anesthetics activate a potent central pain-suppression circuit in the amygdala. Nat Neurosci 23:854–868.

Janak PH, Tye KM (2015) From circuits to behaviour in the amygdala. Nature 517 517:284–292.

Kargl D, Kaczanowska J, Ulonska S, Groessl F, Piszczek L, Lazovic J, Buehler K, Haubensak W (2020) The amygdala instructs insular feedback for affective learning. Elife 9:e60336.

Kim J, Zhang X, Muralidhar S, LeBlanc SA, Tonegawa S (2017) Basolateral to central amygdala neural circuits for appetitive behaviors. Neuron 93:1464–1479.

Lee HJ, Groshek F, Petrovich GD, Cantalini JP, Gallagher M, Holland PC (2005) Role of amygdalo-nigral circuitry in conditioning of a visual stimulus paired with food. J Neurosci 25:3881–3888.

Li H, Penzo MA, Taniguchi H, Kopec CD, Huang ZJ, Li B (2013) Experience-dependent modification of a central amygdala fear circuit. Nat Neurosci 16:332–339.

Lu J, Li C, Singh-Alvarado J, Zhou ZC, Fröhlich F, Mooney R, Wang F (2018) MIN1PIPE: a miniscope 1-photon-based calcium imaging signal extraction pipeline. Cell Rep 23:3673–3684.

McDannald M, Kerfoot E, Gallagher M, Holland PC (2004) Amygdala central nucleus function is necessary for learning but not expression of conditioned visual orienting. Eur J Neurosci 20:240–248.

Miri A, Daie K, Burdine RD, Aksay E, Tank DW (2011) Regression-based identification of behavior-encoding neurons during large-scale optical imaging of neural activity at cellular resolution. J Neurophysiol 105:964–980.

Ozawa T, Ycu EA, Kumar A, Yeh LF, Ahmed T, Koivumaa J, Johansen JP (2017) A feedback neural circuit for calibrating aversive memory strength. Nat Neurosci 20:90–97.

Pare D, Duvarci S (2012) Amygdala microcircuits mediating fear expression and extinction. Curr Opin Neurobiol 22:717–723.

Pare D, Quirk GJ (2017) When scientific paradigms lead to tunnel vision: lessons from the study of fear. NPJ Sci Learn 2:6.

Penzo MA, Robert V, Tucciarone J, De Bundel D, Wang M, Van Aelst L, Darvas M, Parada LF, Palmiter RD, He M, Huang ZJ, Li B (2015) The paraventricular thalamus controls a central amygdala fear circuit. Nature 519:455–459.

Sejnowski TJ (1999) The book of Hebb. Neuron 24:773–776.

Sheintuch L, Rubin A, Brande-Eilat N, Geva N, Sadeh N, Pinchasof O, Ziv Y (2017) Tracking the same neurons across multiple days in Ca2+ imaging data. Cell Rep 21:1102–1115.

Soriano P (1999) Generalized lacZ expression with the ROSA26 Cre reporter strain. Nat Genet 21:70–71.

Stern SA, Doerig KR, Azevedo EP, Stoffel E, Friedman JM (2018) Control of non-homeostatic feeding in sated mice using associative learning of contextual food cues. Mol Psychiatry 25:666–679.

Wilensky AE, Schafe GE, Kristensen MP, Ledoux JE (2006) J Neurosci 26:12387–12396.

Wilson TD, Valdivia S, Khan A, Ahn HS, Adke AP, Gonzalez SM, Sugimura YK, Carrasquillo Y (2019) Dual and opposing functions of the central amygdala in the modulation of pain. Cell Rep 29:332–346.e5.

Yu K, da Silva PG, Albeanu DF, Li B (2016) Central amygdala somatostatin neurons gate passive and active defensive behaviors. J Neurosci 36:6488–6496.

Yu K, Ahrens S, Zhang X, Schiff H, Ramakrishnan C, Fenno L, Deisseroth K, Zhao F, Luo MH, Gong L, He M, Zhou P, Paninski L, Li B (2017) The central amygdala controls learning in the lateral amygdala. Nat Neurosci 20:1680–1685.